

# FMM-accelerated solvers for the Laplace-Beltrami problem on complex surfaces in three dimensions

Dhwanit Agarwal<sup>1</sup>  
*University of Texas at Austin*  
*Austin, TX, 78712*  
dhwanit@oden.utexas.edu

Michael O'Neil<sup>2</sup>  
*Courant Institute, NYU*  
*New York, NY 10012*  
oneil@cims.nyu.edu

Manas Rachh  
*Center for Computational Mathematics, Flatiron Institute*  
*New York, NY 10010*  
mrachh@flatironinstitute.org

November 30, 2021

---

<sup>1</sup>Research supported by UT-Austin CoLab and UTEN Partnership, Portuguese Science and Technology Foundation under funding #201801976/UTA18-001217.

<sup>2</sup>Research supported in part by the Office of Naval Research under award numbers #N00014-17-1-2451 and #N00014-18-1-2307, and the Simons Foundation/SFARI (560651, AB).

## Abstract

The Laplace-Beltrami problem on closed surfaces embedded in three dimensions arises in many areas of physics, including molecular dynamics (surface diffusion), electromagnetics (harmonic vector fields), and fluid dynamics (vesicle deformation). Using classical potential theory, the Laplace-Beltrami operator can be pre-/post-conditioned with integral operators whose kernel is translation invariant, resulting in well-conditioned Fredholm integral equations of the second-kind. These equations have the standard  $1/r$  kernel from potential theory, and therefore the equations can be solved rapidly and accurately using a combination of fast multipole methods (FMMs) and high-order quadrature corrections. In this work we detail such a scheme, presenting two alternative integral formulations of the Laplace-Beltrami problem, each of whose solution can be obtained via FMM acceleration. We then present several applications of the solvers, focusing on the computation of what are known as *harmonic vector fields*, relevant for many applications in electromagnetics. A battery of numerical results are presented for each application, detailing the performance of the solver in various geometries.

**Keywords:** Nyström method, Laplace-Beltrami, harmonic vector field, fast multipole method, potential theory.

## Contents

<b>1</b>	<b>Introduction</b>	<b>2</b>
<b>2</b>	<b>The Laplace-Beltrami problem</b>	<b>3</b>
<b>3</b>	<b>Integral formulation</b>	<b>4</b>
<b>4</b>	<b>An FMM-accelerated solver</b>	<b>6</b>
<b>5</b>	<b>Harmonic vector fields</b>	<b>7</b>
<b>6</b>	<b>Numerical examples</b>	<b>8</b>
6.1	Numerical second-kindness . . . . .	8
6.2	Order of convergence . . . . .	10
6.3	An alternative integral equation . . . . .	10
6.4	Harmonic fields . . . . .	12
<b>7</b>	<b>Conclusions and future work</b>	<b>14</b>

# 1 Introduction

The Laplace-Beltrami problem along surfaces in three dimensions appears in many fields, including plasma physics [34], fluid mechanics [40,44], electromagnetics [13–15,35], surface diffusion, pattern formation [26,39], and computational geometry [29]. In general, the Laplace-Beltrami operator is a 2nd-order variable coefficient elliptic operator whose behavior is highly dependent on the nature of the surface on which it is defined. Its eigenfunctions are useful in describing band-limited functions defined along the associated manifold or surface, and more generally, the related harmonic vector fields provide a basis for important classes of functions appearing in electromagnetics (e.g. non-radiating currents, etc.).

To this end, suppose that  $\Gamma$  is at least a twice-differentiable surface without boundary embedded in  $\mathbb{R}^3$ . Let  $\nabla_\Gamma$  denote the intrinsic surface gradient, and let its adjoint acting on the space of continuously differentiable  $\mathbb{L}^2$  tangential vector fields on the boundary, denoted by  $\nabla_\Gamma \cdot$ , be the intrinsic surface divergence. Given a mean-zero function  $f$  defined along  $\Gamma$ , the Laplace-Beltrami problem is to find a mean-zero function  $u$  satisfying  $\Delta_\Gamma u = f$ , where  $\Delta_\Gamma$  is the Laplace-Beltrami operator defined as  $\Delta_\Gamma = \nabla_\Gamma \cdot \nabla_\Gamma$ . The mean-zero condition on  $f$  and  $u$  is required for unique solvability due to a rank-deficiency of the Laplace-Beltrami operator [13,35,37].

In many of the applications discussed above, the Laplace-Beltrami problem naturally arises for the computation of the Hodge decomposition of tangential vector fields. Any smooth tangential vector field  $\mathbf{F}$  on the surface  $\Gamma$  can be written as

$$\mathbf{F} = \nabla_\Gamma \alpha + \mathbf{n} \times \nabla_\Gamma \beta + \mathbf{H}, \quad (1.1)$$

where  $\alpha, \beta$  are smooth functions on  $\Gamma$ ,  $\mathbf{H}$  is a harmonic field satisfying  $\nabla_\Gamma \cdot \mathbf{H} = \nabla_\Gamma \cdot \mathbf{n} \times \mathbf{H} = 0$ , and  $\mathbf{n}$  is the unit normal to the surface  $\Gamma$ . The curl free component  $\nabla_\Gamma \alpha$  and the divergence free component  $\mathbf{n} \times \nabla_\Gamma \beta$  can be computed via the solution of the following two Laplace-Beltrami problems:

$$\Delta_\Gamma \alpha = \nabla_\Gamma \cdot \mathbf{F}, \quad \Delta_\Gamma \beta = -\nabla_\Gamma \cdot (\mathbf{n} \times \mathbf{F}). \quad (1.2)$$

A related problem is that of determining a basis for harmonic vector fields on non-contractible surfaces, which plays a crucial role for several integral representations in computational electromagnetics. On a genus  $g$  object, the space of harmonic vector fields forms a  $2g$ -dimensional vector space. One can compute elements of this basis via the solution of the two Laplace-Beltrami problems above for a randomly generated smooth vector field  $\mathbf{F}$ , which with high probability tends to have a non-trivial projection onto the subspace of harmonic vector fields.

Numerical methods for the Laplace-Beltrami problem can be typically classified into two categories. The first category of methods rely on the direct discretization of the differential operator on surface. Examples include finite element methods [1,4,6,10], virtual element methods [2,19], differencing methods [48], and level set methods [3,7,23,32,33]. The level set methods differ from the rest of the direct discretizations of the PDE as they rely on using an embedded finite difference grid in the volume  $\mathbb{R}^3$  to discretize a thickening of the surface.

On the other hand, the other general category of methods is to reformulate the Laplace-Beltrami problem as an integral equation along the surface. For example, on a flat surface the Laplace-Beltrami operator reduces to the standard Laplace operator and therefore the Green's function is known to be  $G(\mathbf{x}) = -\log |\mathbf{x}|/(2\pi)$ . This Green's function  $G$  can be used as a parametrix for the fundamental solution to the Laplace-Beltrami operator on general surfaces as well [30]. This idea has also been used for the solution of the related Yukawa-Beltrami problem on general surfaces, including surfaces with boundary in [31]. A separation of variables approach, combined with an integral reformulation

of an ODE, is presented in [20]; this approach was also shown to be applicable in geometries with edges. An alternate integral equation based approach is to use the Green's function of the free-space Laplace equation in three dimensions as either left or right preconditioners for the Laplace-Beltrami problem [37].

In this work, we present a fast multipole method (FMM) accelerated iterative solver for the solution of the Laplace-Beltrami problems on complex three-dimensional surfaces based on the integral formulation presented in [37], and using the locally corrected quadrature approach of [21]. In some respects, this work can be considered *Part II* of the earlier work [37]. The primary motivation of choosing this approach is two-fold: (1) the resulting integral equations tend to be as well-conditioned as the underlying physical problem (which is quite well-conditioned, in an absolute sense), and (2) since the representation uses layer potentials related to the free space Green's function in three dimensions, the numerical solver can be coupled to existing optimized FMM libraries [21,22]. We demonstrate the well-conditioned nature of the integral equation through a battery of numerical experiments, each of which incorporates a high-order representation of the surface and high-order quadratures. We also show the importance of what we refer to as *numerical second-kindness* when discretizing the integral equation using locally corrected quadrature methods. These methods rely on the accurate computation of the principal-value part of the layer potentials in the representation. In particular, while there are several equivalent integral formulations of the same PDE on the surface, we show that the formulation which explicitly handles the identity term of the integral equation tends to be the most stable (from a numerical point of view). Lastly, with the acceleration provided by FMMs, our integral formulation can be used to compute a basis for harmonic vector fields in relatively high-genus geometries.

The rest of the paper is organized in follows. In Section 2, we describe the Laplace-Beltrami problem. In Section 3, we review the integral equation formulation presented in [37], and in Section 4, we review a high order FMM-accelerated iterative solver. In Section 5, we discuss an application of the solver to the computation of a basis for harmonic vector fields on non-contractible surfaces. In Section 6, we present several numerical examples to demonstrate the efficiency of our approach, including a discussion on the importance of numerical second-kindness. Finally, in Section 7, we conclude by discussing avenues for future research.

## 2 The Laplace-Beltrami problem

The Laplace-Beltrami operator, also known as the surface Laplacian, is the generalization of the Laplace operator to general (smooth) manifolds. In this work, we will focus on smooth surfaces embedded in three dimensions. Suppose  $\Gamma \subset \mathbb{R}^3$  is an oriented surface with at least two continuous derivatives, and let  $\mathbf{x}(u, v) : D \subset \mathbb{R}^2 \rightarrow \mathbb{R}^3$  denote a local parametrization of  $\Gamma$ . The first fundamental form, or equivalently the metric tensor at  $\mathbf{x}(u, v)$ , is given by

$$g = \begin{bmatrix} g_{11} & g_{12} \\ g_{21} & g_{22} \end{bmatrix} = \begin{bmatrix} \partial_u \mathbf{x} \cdot \partial_u \mathbf{x} & \partial_u \mathbf{x} \cdot \partial_v \mathbf{x} \\ \partial_v \mathbf{x} \cdot \partial_u \mathbf{x} & \partial_v \mathbf{x} \cdot \partial_v \mathbf{x} \end{bmatrix}, \quad (2.1)$$

where  $\partial_u \mathbf{x}$  and  $\partial_v \mathbf{x}$  are abbreviations for  $\frac{\partial \mathbf{x}}{\partial u}$  and  $\frac{\partial \mathbf{x}}{\partial v}$  respectively and are the tangents to the surface at  $\mathbf{x} \in \Gamma$ . The unit normal at  $\mathbf{x}$  can be written as

$$\mathbf{n}(\mathbf{x}) = \frac{\partial_u \mathbf{x} \times \partial_v \mathbf{x}}{|\partial_u \mathbf{x} \times \partial_v \mathbf{x}|}. \quad (2.2)$$

The unit vectors in the directions of  $\partial_u \mathbf{x}$ ,  $\partial_v \mathbf{x}$ , and  $\mathbf{n}(\mathbf{x})$  form a local coordinate system (not necessarily orthogonal) at each point  $\mathbf{x} \in \Gamma$ .

Next, suppose that  $\mathbf{F}$  is a smooth tangential vector field defined along  $\Gamma$  and is expressed in terms of the local tangent vectors  $\partial_u \mathbf{x}$ ,  $\partial_v \mathbf{x}$  as

$$\mathbf{F}(u, v) = F_1 \partial_u \mathbf{x} + F_2 \partial_v \mathbf{x} . \quad (2.3)$$

The surface divergence of  $\mathbf{F}$ , denoted by  $\nabla_\Gamma \cdot \mathbf{F}$  is then [18, 35] given by

$$\nabla_\Gamma \cdot \mathbf{F} = \frac{1}{\sqrt{|g|}} \left( \partial_u \left( \sqrt{|g|} F_1 \right) + \partial_v \left( \sqrt{|g|} F_2 \right) \right) , \quad (2.4)$$

where  $|g|$  is the determinant of the metric tensor  $g$ . The surface gradient operator  $\nabla_\Gamma$ , formally defined as the adjoint of the surface divergence operator on the space of  $\mathbb{L}^2$  functions with respect to the induced metric on  $\Gamma$ , is given by

$$\nabla_\Gamma \psi = \left( g^{11} \partial_u \psi + g^{12} \partial_v \psi \right) \partial_u \mathbf{x} + \left( g^{21} \partial_u \psi + g^{22} \partial_v \psi \right) \partial_v \mathbf{x} , \quad (2.5)$$

where  $\psi = \psi(u, v)$  is a scalar function defined on  $\Gamma$  and  $g^{ij}$  denote the components of the inverse of the metric tensor, denoted by  $g^{-1}$ .

The Laplace-Beltrami operator is then defined as  $\Delta_\Gamma = \nabla_\Gamma \cdot \nabla_\Gamma$ , and is explicitly given by the expression

$$\Delta_\Gamma \psi = \frac{1}{\sqrt{|g|}} \left( \partial_u \left[ \sqrt{|g|} \left( g^{11} \partial_u \psi + g^{12} \partial_v \psi \right) \right] + \partial_v \left[ \sqrt{|g|} \left( g^{21} \partial_u \psi + g^{22} \partial_v \psi \right) \right] \right) . \quad (2.6)$$

The standard Laplace-Beltrami problem is to solve the following PDE for  $\psi$  along  $\Gamma$ ,

$$\Delta_\Gamma \psi = f , \quad (2.7)$$

where  $f$  is a given function. Conditions on the regularity required in  $f$ , and the subsequent regularity obtained in  $\psi$  have been studied in [11, 20, 25, 41]. We will assume that all functions and surfaces are sufficiently smooth so as to obtain high order accuracy in the subsequently numerical examples.

As is clear, the Laplace-Beltrami operator maps constant functions along  $\Gamma$  to zero. Thus, the equation (2.7) is rank-one deficient [24, 43] (and formally self-adjoint). The following lemma [37, 41] summarizes a classical result regarding the well-posedness of the above Laplace-Beltrami problem.

**Lemma 1.** *Let  $\Gamma$  be a smooth, closed, and orientable boundary. Along  $\Gamma$ , the Laplace-Beltrami operator is uniquely invertible as a map from  $\mathbb{M}_0 \rightarrow \mathbb{M}_0$ , the space of mean-zero functions defined on  $\Gamma$ ,*

$$\mathbb{M}_0 = \left\{ \psi : \int_\Gamma \psi \, da = 0 \right\} . \quad (2.8)$$

*Indeed, if the function  $f$  defined along  $\Gamma$  has mean zero, then there exists a unique mean-zero solution,  $\psi$ , to the Laplace-Beltrami problem  $\Delta_\Gamma \psi = f$ .*

### 3 Integral formulation

In this section, we review an equivalent well-conditioned second-kind integral equation for the solution of the Laplace-Beltrami problem. This formulation relies on preconditioning the Laplace-Beltrami operator on both the left and right using the Laplace single layer potential. The resulting

Fredholm operator can be expressed in terms of standard layer potentials for the free space Laplace equation in three dimensions.

Before describing this formulation, we first define the relevant layer potentials used in the formulation. The Green's function  $G$  for Laplace's equation in three dimensions given by

$$G(\mathbf{x}, \mathbf{y}) = \frac{1}{4\pi|\mathbf{x} - \mathbf{y}|}. \quad (3.1)$$

The single and double layer potentials are then given by:

$$\mathcal{S}[\sigma](\mathbf{x}) = \int_{\Gamma} G(\mathbf{x}, \mathbf{y}) \sigma(\mathbf{y}) da, \quad \mathcal{D}[\mu](\mathbf{x}) = \int_{\Gamma} (\nabla_{\mathbf{y}} G(\mathbf{x}, \mathbf{y}) \cdot \mathbf{n}(\mathbf{y})) \mu(\mathbf{y}) da. \quad (3.2)$$

When the *target* point  $\mathbf{x}$  lies on  $\Gamma$ , the integral defining the double layer should be interpreted in a principal value sense. For smooth surfaces  $\Gamma$ , both  $\mathcal{S}$  and  $\mathcal{D}$  are compact operators as maps from  $\mathbb{L}^2(\Gamma) \rightarrow \mathbb{L}^2(\Gamma)$ . Related to the single and double layer potentials are the restrictions of their normal derivatives to  $\Gamma$  given by

$$\begin{aligned} \mathcal{S}'[\sigma](\mathbf{x}) &= \mathbf{n}(\mathbf{x}) \cdot \nabla \int_{\Gamma} G(\mathbf{x}, \mathbf{y}) \sigma(\mathbf{y}) da, \\ \mathcal{D}'[\mu](\mathbf{x}) &= \int_{\Gamma} \mathbf{n}(\mathbf{x}) \cdot \nabla_{\mathbf{x}} \nabla_{\mathbf{y}} G(\mathbf{x}, \mathbf{y}) \cdot \mathbf{n}(\mathbf{y}) \mu(\mathbf{y}) da. \end{aligned} \quad (3.3)$$

The integral defining  $\mathcal{S}'$  is to be interpreted in a principal value sense, and that for  $\mathcal{D}'$  is to be interpreted in a finite-part sense [28, 35]. The operator  $\mathcal{S}'$  is also a compact operator on  $\mathbb{L}^2(\Gamma)$ , whereas  $\mathcal{D}'$  is a hypersingular operator.

Finally, let  $\mathcal{S}''$  denote the restriction of the second normal derivative of  $\mathcal{S}$  to  $\Gamma$  given by:

$$\mathcal{S}''[\sigma](\mathbf{x}) = \int_{\Gamma} (\mathbf{n}(\mathbf{x}) \cdot \nabla_{\mathbf{x}} \nabla_{\mathbf{x}} G(\mathbf{x}, \mathbf{y}) \cdot \mathbf{n}(\mathbf{x})) \sigma(\mathbf{y}) da, \quad (3.4)$$

where, as for the integral defining  $\mathcal{D}'$ , the integral should be interpreted in a finite-part sense [28, 35, 37]. It can be shown that the *difference* operator  $\mathcal{S}'' + \mathcal{D}'$  is a compact operator on  $\mathbb{L}^2(\Gamma)$  [35], as the dominant singularities in the integrand cancel each other out.

In the following theorem, we now review the equivalent second-kind boundary integral equation presented in [37], for the solution of the Laplace-Beltrami equation (2.7).

**Theorem 1.** *Suppose that  $f$  is a mean-zero function in  $\mathbb{L}^2(\Gamma)$ . Then there exists a unique solution  $\sigma$  in  $\mathbb{L}^2(\Gamma)$  which satisfies*

$$-\frac{\sigma}{4} + \mathcal{D}^2[\sigma] - \mathcal{S}(\mathcal{S}'' + \mathcal{D}' - 2HS')[\sigma] + \mathcal{S}\mathcal{W}\mathcal{S}[\sigma] = \mathcal{S}[f], \quad (3.5)$$

and  $\int_{\Gamma} \mathcal{S}[\sigma] da = 0$ . Here  $H$  is the mean curvature along  $\Gamma$ , and  $\mathcal{W}$  is the operator given by

$$\mathcal{W}[\sigma] = \frac{1}{|\Gamma|} \int_{\Gamma} \sigma da. \quad (3.6)$$

Furthermore,  $\psi = \mathcal{S}[\sigma]$  is the unique mean-zero solution to  $\Delta_{\Gamma}\psi = f$ .

A proof of this result can be found in [37].

## 4 An FMM-accelerated solver

In this section, we briefly describe the details of our numerical solver for integral equation formulations of the Laplace-Beltrami problem. A full detailed discussion would merely be a reproduction of much of the content of [21], which presents a FMM-accelerated library of solvers for various boundary integral equations. Our numerical solver is based on the software packages `fmm3dbie` [17] and `FMM3D` [16]; subsequently, examples for the Laplace-Beltrami problem will be included in the package `fmm3dbie`. We now give a very brief overview of the solver, and make a few remarks which are specific to the Laplace-Beltrami problem.

For simplicity, consider a second-kind integral equation of the form

$$\sigma(\mathbf{x}) + \int_{\Gamma} K(\mathbf{x}, \mathbf{x}') \sigma(\mathbf{x}') da(\mathbf{x}') = f(\mathbf{x}) \quad \mathbf{x} \in \Gamma, \quad (4.1)$$

where  $K(\mathbf{x}, \mathbf{x}')$  is either  $G(\mathbf{x}, \mathbf{x}')$  or one of its directional derivatives. Suppose that the surface  $\Gamma$  is represented via a disjoint union of patches  $\Gamma_j$ ,  $\Gamma = \cup_{j=1}^{N_{\text{patches}}} \Gamma_j$  and that each patch  $\Gamma_j$  is parametrized by a non-degenerate chart  $\mathbf{X}^j : T_0 \rightarrow \Gamma_j$ , where  $T_0$  is the standard simplex given by

$$T_0 = \{(u, v) : u \geq 0, v \geq 0, u + v \leq 1\} \subset \mathbb{R}^2.$$

An order  $p$  discretization of  $\Gamma$  is one where the components of  $\mathbf{X}^j$ ,  $\partial_u \mathbf{X}^j$ , and  $\partial_v \mathbf{X}^j$  are represented by a polynomial expansion of total degree less than  $p$  on  $T_0$ . One way to obtain such a representation is to sample the chart and the derivative information at order  $p$  Vioreanu-Rokhlin nodes [47] which are stable interpolation nodes for orthogonal polynomials [5, 27] on  $T_0$ .

**Remark 1.** *Triangulations of surfaces obtained from CAD or standard meshing packages often tend to be low order and introduce several artificial edges and corners on the discretized surface. In our examples, with the aim of showing high-order convergence, we use the surface smoothing algorithm discussed in [46] to convert these low-order triangulations of complex geometries to arbitrarily high order triangulations of a nearby related  $C^\infty$  surface. In some of our examples, analytic parameterizations of the domains are known and are used instead of the algorithm of [46]. The algorithm was only applied to complex geometries, such as the multi-holed object in Figure 3.*

Let  $\{\mathbf{x}_i\}_{i=1}^N$  denote the union of the samples of the charts  $\mathbf{X}^j$  at the Vioreanu-Rokhlin nodes of order  $p$ . A Nyström discretization of Equation (4.1) is given by

$$\sigma_i + w_{ii}\sigma_i + \sum_{j \neq i} w_{ij} K(\mathbf{x}_i, \mathbf{x}_j) \sigma_j = f(\mathbf{x}_i), \quad (4.2)$$

where  $\sigma_i$  is an approximation for the solution  $\sigma(\mathbf{x}_i)$ . In [21], the layer potential  $\int_{\Gamma} K(\mathbf{x}_i, \mathbf{x}') \sigma(\mathbf{x}') da(\mathbf{x}')$  for  $\mathbf{x}_i \in \Gamma_\ell$  is approximated using a combination of generalized Gaussian quadrature for the contribution of  $\Gamma_\ell$  to the layer potential, adaptive integration for patches  $\Gamma_j$  which are close to  $\mathbf{x}_i$  and target independent oversampled quadratures for all the remaining patches. Let  $\{s_i, w_i\}_{i=1}^{N_{\text{over}}}$  denote the oversampled quadrature nodes and weights for integrating smooth functions on  $\Gamma$ , then the Nyström discretization in Equation (4.2) takes the form

$$\sigma_i + w_{ii}\sigma_i + \sum_{j=1}^{n_i} w_{ij} K(\mathbf{x}_i, \mathbf{y}_{ij}) \tilde{\sigma}_{ij} + \sum_{\substack{j=1 \\ s_j \in \text{Far}(\mathbf{x}_i)}}^{N_{\text{over}}} w_j K(\mathbf{x}_i, s_j) \tilde{\sigma}_j = f(\mathbf{x}_i), \quad (4.3)$$

where  $\tilde{\sigma}_j$  and  $\tilde{\sigma}_{ij}$  are the interpolated values of  $\sigma(\mathbf{x}_i)$  at  $\mathbf{s}_j$  and  $\mathbf{y}_{ij}$ , respectively, obtained via local polynomial interpolation of the samples  $\sigma_i$ , and  $\mathbf{y}_{ij}$ ,  $w_{ij}$  are the quadrature nodes and weights (which can be precomputed and stored) used in the adaptive integration procedure to accurately compute the contribution of the layer potential due to self panel  $\Gamma_\ell$  and the near panels at the target location  $\mathbf{x}_i$ . There are  $O(1)$  patches which are in the near field of each target, and since the far field part of the layer potential is computed using a target independent quadrature rule, the corresponding contribution can be computed using standard fast multipole methods [21, 22]. If Equation (4.3) is well-conditioned, then we can obtain the solution  $\sigma_i$  in  $O(N)$  time using an iterative algorithm such as GMRES [42].

In the context of solving the Laplace-Beltrami problem, there are two details that aren't already a part of the `fmm3dbie` [17] package: (1) the contribution of  $S'' + \mathcal{D}'$  needs to be handled as a single operator since both  $S''$  nor  $\mathcal{D}'$  are hypersingular operators, but their sum  $S'' + \mathcal{D}'$  is a compact operator of order  $-1$ , and (2) the mean curvature  $H$  needs to be computed by spectral differentiation of  $\partial_u X^j$  and  $\partial_v X^j$ .

## 5 Harmonic vector fields

For a surface  $\Gamma$  with unit normal  $\mathbf{n}$ , a harmonic vector field  $\mathbf{H}$  is one which satisfies

$$\nabla_\Gamma \cdot \mathbf{H} = 0, \quad \nabla_\Gamma \cdot (\mathbf{n} \times \mathbf{H}) = 0. \quad (5.1)$$

On a genus  $g$  surface, it is well known that the space of harmonic vector fields is  $2g$  dimensional [9, 11, 12]. Moreover, it follows from the definition that if  $\mathbf{H}$  is a harmonic vector field, then  $\mathbf{n} \times \mathbf{H}$  is also a harmonic vector field which is linearly independent of  $\mathbf{H}$ . Any tangential  $C^1$  vector field  $\mathbf{F}$  along a smooth surface admits a Hodge decomposition [11, 12]:

$$\mathbf{F} = \nabla_\Gamma \alpha + \mathbf{n} \times \nabla_\Gamma \beta + \mathbf{H}, \quad (5.2)$$

where  $\alpha$  and  $\beta$  are scalar functions defined on the surface  $\Gamma$  and  $\mathbf{H}$  is a harmonic vector field. Given a smooth tangential vector field  $\mathbf{F}$ , one can use the existence of this decomposition to compute linearly independent harmonic vector fields  $\mathbf{H}$  by solving the following Laplace-Beltrami equations and subsequently computing  $\mathbf{H}$ :

$$\begin{aligned} \Delta_\Gamma \alpha &= \nabla_\Gamma \cdot \mathbf{F}, \quad \Delta_\Gamma \alpha = -\nabla_\Gamma \cdot (\mathbf{n} \times \mathbf{F}), \\ \mathbf{H} &= \mathbf{F} - \nabla_\Gamma \alpha - \mathbf{n} \times \nabla_\Gamma \beta. \end{aligned} \quad (5.3)$$

A convenient way of choosing such smooth vector fields  $\mathbf{F}$  is to first define  $\mathbf{V} \in \mathbb{R}^3$  where each component is a low degree random polynomial, and then set  $\mathbf{F} = \mathbf{n} \times \mathbf{n} \times \mathbf{V}$ . The maximum degree of Legendre polynomials should be at least  $\lceil (2g)^{1/3} \rceil$  so that dimension of the space of polynomials is greater than the dimension of the space of the vector fields. For the examples in this paper, we choose the degree to be  $\lceil (2g)^{1/3} \rceil + 3$ . Moreover, suppose that  $\Gamma$  is contained in  $(-L, L)^3$ , then each component is defined to be a scaled tensor product Legendre polynomial [36]  $P_\ell(x/2L)P_m(y/2L)P_n(z/2L)$ , where  $P_n(x)$  is the standard Legendre polynomials of degree  $n$  on  $[-1, 1]$ . The extra factor of 2 in the choice of Legendre polynomials is to avoid requiring additional degrees of freedom to represent  $\mathbf{F}$  on the surface due to large gradients of the Legendre polynomials near the end points  $-1$  and  $1$ .

With high probability, different random polynomial vector fields  $\mathbf{F}$  result in different projections on the different elements of the  $2g$ -dimensional space of vector fields. It is easy to show that if  $\mathbf{H}$  is



a harmonic vector field then  $\mathbf{n} \times \mathbf{H}$  is also a harmonic vector field which is linearly independent of  $\mathbf{H}$ . Thus, in practice one can construct a basis for the harmonic vector field subspace by computing  $\mathbf{H}$  for  $g$  different vector fields  $\mathbf{F}$ , and the remaining  $g$  vector fields of the basis are defined as  $\mathbf{n} \times \mathbf{H}$ .

## 6 Numerical examples

In this section, we provide several numerical examples demonstrating the accuracy and computational efficiency of our solver for the Laplace-Beltrami problem, as well as an application of the solver for computing harmonic vector fields.

### 6.1 Numerical second-kindness

We first turn our attention to the differences in numerical discretizations of the following three (mathematically equivalent) formulations of an integral equation for the Laplace-Beltrami PDE:

$$\mathcal{S}\Delta_{\Gamma}\mathcal{S} = (\mathcal{S}\nabla_{\Gamma}\cdot)(\nabla_{\Gamma}\mathcal{S}) \quad (6.1a)$$

$$= (\nabla_{\Gamma}\cdot\mathcal{S})(\nabla_{\Gamma}\mathcal{S}) \quad (6.1b)$$

$$= -\frac{1}{4}\mathcal{I} + \mathcal{D}^2 - \mathcal{S}(\mathcal{S}'' + \mathcal{D}' - 2\mathcal{H}\mathcal{S}') . \quad (6.1c)$$

For convenience of exposition, we have dropped the rank-one operator  $\mathcal{W}$  as it is not relevant to the discussion in this section. While the above operators (Eq. (6.1a), (6.1b), (6.1c)) are all equal as maps on smooth functions on  $\Gamma$ , their performance when discretized numerically differs significantly on patch-based discretizations of the surface.

The first approach in Equation (6.1a) of composing  $\mathcal{S}\nabla_{\Gamma}\cdot$  with  $\nabla_{\Gamma}\mathcal{S}$  is extremely unstable on patch-based discretizations where smooth functions are represented as independent polynomial expansion on each patch. The discretization does not enforce any smoothness constraint on functions across the patch interfaces which results in a spurious null space proportional to the number of degrees of freedom used to discretize the problem. In particular, the surface divergence is computed after projecting the values of  $\nabla_{\Gamma}\mathcal{S}$  onto a truncated Koornwinder polynomial expansion. On each patch, the surface divergence operator has a null space proportional to the order of the discretization. To circumvent this issue, one could use discretizations commonly used in finite element methods which preserve smoothness of functions across patches. Equation (6.1b) is an equivalent formulation which avoids this issue.

Even though Equation (6.1b) avoids the spurious null-space issue, both Equations (6.1a) and (6.1b) tend to perform poorly when using iterative solver (as compared to using Equation (6.1c)). One of the key reasons for this difference is that *any* numerical discretization of integral operators is inherently compact since the operator is approximated via a finite-rank one. This results in the spectrum of the discretized integral operator clustering closely to the origin, resulting in numerical conditioning issues. Explicitly adding the identity term, as is the case in Equation (6.1c), results in the spectrum of the discretized integral operator clustering at  $-1/4$ . This *greatly* enhances the convergence of iterative methods such as GMRES [42]. These differences in behavior can be demonstrated by applying each of the operators on the right-hand sides of Equation (6.1) to a function whose Laplace-Beltrami signature is known explicitly. On the unit sphere, for a function  $u$  given in terms of its spherical harmonic expansion

$$u = \sum_{n=1}^2 \sum_{m=0}^n c_{nm} Y_{nm}(\theta, \phi), \quad (6.2)$$

where  $Y_{nm}(\theta, \phi)$  are the spherical harmonics of degree  $n$  and order  $m$ , the action of the operator  $\mathcal{S}(\Delta_\Gamma + \mathcal{W})\mathcal{S}$  is diagonal and is given as [45]

$$\begin{aligned} v &= \mathcal{S}(\Delta_\Gamma + \mathcal{W})\mathcal{S}[u] \\ &= - \sum_{n=1}^2 \sum_{m=0}^n c_{nm} \frac{n(n+1)}{(2n+1)^2} Y_{nm}(\theta, \phi). \end{aligned} \quad (6.3)$$

We discretize the layer potentials in representations in Equations (6.1a) to (6.1c) on a unit sphere based on the procedure discussed in Section 4; the unit sphere is discretized using  $N_{\text{patches}}$  number of patches, each of order  $p$ . We then apply these operators to a function  $u$  of the form above. We verify the correctness of our discretization by computing the  $\mathbb{L}^2$  error in the result (compared to the known solution  $v$  above). The coefficients  $c_{nm}$ ,  $n = 1, 2$ ,  $0 \leq m \leq n$  are chosen uniformly from the interval  $(-0.5, 0.5)$ . This error is reported as  $\varepsilon_{mv}$  in Table 1. For all three representations, we note that the error converges to 0 at the expected rate of  $O(h^{p-1})$ .

Next, in order to study the relative performance of these representation in iterative solvers, we compare the spectral properties of the three discretized linear systems. We form the dense matrices for  $N_{\text{patches}} = 192$  and compute their singular value decompositions. The resulting singular values are plotted in Figure 1. As expected, we see that Equation (6.1a) has a large spurious null space and that the other two discretizations are full rank. Moreover, the singular values of Equation (6.1b) cluster at 0, while the singular values of Equation (6.1c) cluster at 0.25. We then solve the Laplace-Beltrami problem  $(\Delta_\Gamma + \mathcal{W})\psi = u$  using each of these discretized linear systems and GMRES. On the right in Figure 1, we plot the estimated residual as a function of iteration number for the three representations. The GMRES residual for Equations (6.1a) and (6.1b) stagnates at the level of discretization error, while Equation (6.1c) is more robust and the residual converges to machine precision independent of discretization error. The analytical solution for the data  $u$  expressed as a spherical harmonic expansions is known to be

$$\begin{aligned} \psi &= (\Delta_\Gamma + \mathcal{W})^{-1}u \\ &= - \sum_{n=1}^2 \sum_{m=0}^n \frac{c_{nm}}{n(n+1)} Y_{nm}(\theta, \phi). \end{aligned} \quad (6.4)$$

In Table 1, we report the  $\mathbb{L}^2$  error in the computed solution  $\psi$ , denoted by  $\varepsilon_s$ . For Equations (6.1b) and (6.1c), the error converges to 0 at the expected rate of  $O(h^{p-1})$  (even though GMRES stagnates at

Representation	$N_{\text{patches}}$	$N$	$\varepsilon_{mv}$	$\varepsilon_s$
Equation (6.1a)	48	480	$3.1 \times 10^{-2}$	$1.1 \times 10^{12}$
	192	1920	$6.8 \times 10^{-3}$	$4.6 \times 10^{10}$
	768	7680	$9.0 \times 10^{-4}$	$3.0 \times 10^7$
Equation (6.1b)	48	480	$1.6 \times 10^{-2}$	$2.2 \times 10^{-1}$
	192	1920	$1.4 \times 10^{-3}$	$3.7 \times 10^{-2}$
	768	7680	$1.8 \times 10^{-4}$	$2.3 \times 10^{-3}$
Equation (6.1c)	48	480	$8.5 \times 10^{-3}$	$8.1 \times 10^{-3}$
	192	1920	$6.3 \times 10^{-4}$	$6.1 \times 10^{-4}$
	768	7680	$8.1 \times 10^{-5}$	$8.0 \times 10^{-5}$

Table 1: Comparison of error in applying  $\mathcal{S}(\Delta_\Gamma + \mathcal{W})\mathcal{S}$  (denoted by  $\varepsilon_{mv}$ ) and inverting  $\Delta_\Gamma + \mathcal{W}$  (denoted by  $\varepsilon_s$ ) for the three equivalent representations given in Equations (6.1a) to (6.1c) on the unit sphere.

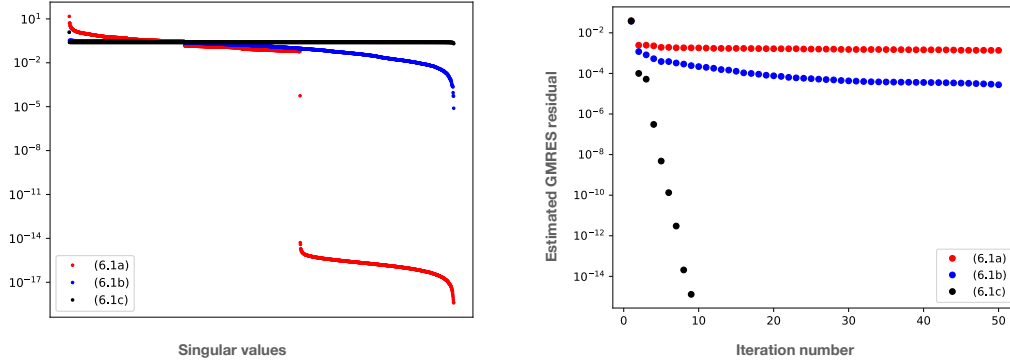


Figure 1: The singular values of the matrices for the three representations Equations (6.1a) to (6.1c) for a sphere discretized with  $N_{\text{patches}} = 192$ , and  $p = 4$  (left) and estimated GMRES residual as a function of iteration number (right).

discretization error for Equation (6.1b)), while for Equation (6.1a), the spurious null space completely pollutes the solution.

## 6.2 Order of convergence

Next, we demonstrate the accuracy and convergence of our solver following the representation in Equation (6.1c). To this end, we use the solver to compute a numerical solution of Laplace-Beltrami equation on a torus with major radius  $R = 2.25$  and minor radius  $r = 0.75$  and compare it with the known analytical solution. Suppose that the torus is parameterized as

$$\mathbf{X}(s, t) = \begin{pmatrix} (R + r \cos t) \cos s \\ (R + r \cos t) \sin s \\ r \sin t \end{pmatrix}, \quad \text{for } s, t \in [0, 2\pi]. \quad (6.5)$$

A simple calculation shows that for this geometry,

$$\begin{aligned} (\Delta_\Gamma + \mathcal{W})z &= \frac{z}{r^2 \sqrt{x^2 + y^2}} \left( R - 2\sqrt{x^2 + y^2} \right) \\ &= \alpha(x, y, z). \end{aligned} \quad (6.6)$$

Next, suppose that the torus is discretized with  $N_{\text{patches}}$  patches, each of order  $p$ , resulting in  $N = N_{\text{patches}} \cdot p(p + 1)/2$  discretization points. We compute the numerical solution  $\psi$  to the Laplace-Beltrami problem  $(\Delta_\Gamma + \mathcal{W})\psi = \alpha$ , with  $\alpha$  defined above, on the torus  $\Gamma$ . In Table 2, we tabulate the numerical results by presenting the error in the computed numerical solution (denoted by  $\varepsilon_s$ ), the estimated rate of convergence  $\rho_c$ , and the mean of the computed solution (denoted by  $\psi_m$ ). We observe expected order convergence to the analytical solution where the observed order is appropriately dependent on the discretization order  $p$  of the patches.

## 6.3 An alternative integral equation

An alternative second-kind integral equation can be derived for the Laplace-Beltrami problem merely by right preconditioning by  $S^2$ . In short, if we let  $\psi = S^2[\sigma]$ , then after a suitable application of

$p$	$N_{\text{patches}}$	$N$	$\varepsilon_s$	$\rho_c$	$\psi_m$
3	100	600	$8.2 \times 10^{-3}$		$1.8 \times 10^{-15}$
3	400	2400	$1 \times 10^{-3}$	3.03	$1.3 \times 10^{-12}$
3	1600	9600	$1.2 \times 10^{-4}$	3.05	$1.3 \times 10^{-12}$
4	100	1000	$1.1 \times 10^{-3}$		$6.3 \times 10^{-13}$
4	400	4000	$1.3 \times 10^{-4}$	3.08	$1.1 \times 10^{-12}$
4	1600	16000	$1.7 \times 10^{-5}$	2.94	$6.4 \times 10^{-14}$
5	100	1500	$6.3 \times 10^{-5}$		$6.3 \times 10^{-11}$
5	400	6000	$2 \times 10^{-6}$	4.97	$1.6 \times 10^{-12}$
5	1600	24000	$6.5 \times 10^{-8}$	4.94	$5.2 \times 10^{-13}$
7	100	2800	$3.3 \times 10^{-7}$		$7.7 \times 10^{-13}$
7	400	11200	$2.9 \times 10^{-9}$	6.83	$1.0 \times 10^{-12}$
7	1600	44800	$1.1 \times 10^{-10}$	4.72	$5.5 \times 10^{-13}$
9	16	720	$4.8 \times 10^{-6}$		$1.1 \times 10^{-14}$
9	64	2880	$1.2 \times 10^{-8}$	8.64	$9.8 \times 10^{-14}$
9	256	11520	$1 \times 10^{-10}$	6.9	$4.2 \times 10^{-13}$

Table 2: Convergence results for  $(\Delta_\Gamma + \mathcal{W})\psi = \alpha$ , with  $\alpha$  defined in Equation (6.6), on a torus with major radius  $R = 2.25$  and minor radius  $r = 0.75$

various Calderón identities [8, 37], the Laplace-Beltrami problem  $(\Delta_\Gamma + \mathcal{W})\psi = f$  is replaced by

$$\left(-\frac{\mathcal{I}}{4} + (S')^2 - (S'' + \mathcal{D}' - 2HS')S + \mathcal{W}S^2\right)[\sigma] = f. \quad (6.7)$$

This formulation is also second-kind, but its compact part differs ever so slightly from that of Equation (6.1c). In Table 3, we compare the two integral representations, Equation (6.1c) and Equation (6.7), with respect to the number of GMRES iterations required and the accuracy in computing  $(\Delta_\Gamma + \mathcal{W})\psi = \alpha$  on the torus. Since the compact part of both the representations don't differ by much, the numerical performance of both these representations is practically indistinguishable.

As can be seen from the results above, there is not any notable difference in solving the Laplace-Beltrami PDE by representing the solution as  $\psi = S[\sigma]$  and preconditioning on the left with another application of  $S$ , or by representing  $\psi = S^2[\sigma]$ , both in terms of the accuracy achieved and the performance of the iterative solvers. However, various applications may dictate one representation over the other. In the context of solving Maxwell's equations or static currents in type I superconductors using the Debye source representation [15], we find that using  $\psi = S^2[\sigma]$  is more faithful to the

$N_{\text{patches}}$	$p$	$N$	$\mathbb{L}^2$ error with $S\Delta_\Gamma S$	# iterations	$\mathbb{L}^2$ error with $\Delta_\Gamma S^2$	# iterations
100	5	1500	6.3 E-5	9	6.5 E-5	10
400	5	6000	2.0 E-6	8	2.0 E-6	8
1600	5	24000	6.5 E-8	8	6.4 E-8	8

Table 3: Comparison of GMRES iteration counts and errors for  $S(\Delta_\Gamma + \mathcal{W})S$  and  $(\Delta_\Gamma + \mathcal{W})S^2$  for a torus with major radius 2.25 and minor radius 0.75.

spectral properties of the solution [13–15]. As a map from mean zero functions to themselves, if  $\Delta_\Gamma \psi = f$  then  $\psi = \Delta_\Gamma^{-1} f$ , which implies that the map from  $f \rightarrow \psi$  is a pseudo-differential operator of order  $-2$ . However, if we represent  $\psi = \mathcal{S}[\sigma]$ , then the map from  $\sigma \rightarrow \psi$  is a pseudo-differential operator of order  $-1$ , while for the representation  $\psi = \mathcal{S}^2[\sigma]$ , the map from  $\sigma \rightarrow \psi$  is indeed a pseudo-differential operator of order  $-2$ . This significantly affects the spectral properties of some of the operators appearing in the generalized-Debye representation.

For example, one of the operators in the Generalized-Debye representation [11] is

$$\mathcal{A}[q] = \mathbf{n} \cdot \nabla \times \mathcal{S}_k [\mathbf{n} \times \nabla_\Gamma \Delta_\Gamma^{-1} q], \quad (6.8)$$

where  $q$  is a mean-zero surface charge and  $\mathcal{S}_k$  is the single-layer potential for the Helmholtz equation [38] with wave number  $k$  given by

$$\mathcal{S}_k[\sigma] = \int_\Gamma \frac{e^{ik|\mathbf{x}-\mathbf{y}|}}{4\pi|\mathbf{x}-\mathbf{y}|} \sigma(\mathbf{y}) da(\mathbf{y}). \quad (6.9)$$

Note that  $\mathcal{A}$  is a pseudo-differential operator of order  $-1$  when acting on  $q$ . If we represent the quantity  $\Delta_\Gamma^{-1} q$  as  $\psi = \mathcal{S}[\sigma]$ , then we need to discretize the following operator instead of  $\mathcal{A}$ ,

$$\tilde{\mathcal{A}}[\sigma] = \mathbf{n} \cdot \nabla \times \mathcal{S}_k [\mathbf{n} \times \nabla_\Gamma \mathcal{S}[\sigma]]. \quad (6.10)$$

It can be shown that  $\tilde{\mathcal{A}}$  is a second-kind Fredholm operator of the form  $-\mathcal{I}/4 + \mathcal{K}$ , for some compact operator  $\mathcal{K}$ , when acting on  $\sigma$  (as opposed to  $\mathcal{A}$  which is itself compact operator). To the best of our knowledge, explicit Calderón identities are not known for this operator. However, one can deduce the second-kindness of the operator and the strength of the identity term by analyzing the action of the operator on spherical harmonics when the boundary is the unit sphere. In particular, if  $\Gamma$  is the unit sphere, then

$$\tilde{\mathcal{A}}[Y_{nm}] = -\frac{ik j_n(k) h_n(k) n(n+1)}{2n+1} Y_{nm} = c_n Y_{nm}, \quad (6.11)$$

where  $j_n$  and  $h_n$  are the spherical Bessel and Hankel functions of order  $n$  respectively. This result can be derived using the results in [45] for example. From the asymptotic expressions of spherical Bessel and Hankel functions, it follows that  $c_n = -1/4 + O(1/n)$  as  $n \rightarrow \infty$ . Not handling the identity term explicitly can affect the performance of quadrature methods (such as Generalized Gaussian quadrature which is the method used in `fmm3dbie`) as these methods rely on discretizing just the principal value parts of operators. No such issue arises when  $\Delta_\Gamma^{-1} q$  is replaced with  $\mathcal{S}^2[\sigma]$ .

## 6.4 Harmonic fields

Now we present the numerical results for the computation of the harmonic vector fields on a twisted torus geometry whose boundary  $\Gamma$  is parametrized by  $\mathbf{X} : [0, 2\pi]^2 \rightarrow \Gamma$  with

$$\mathbf{X}(u, v) = \sum_{i=-1}^2 \sum_{j=-1}^2 \delta_{i,j} \begin{pmatrix} \cos v \cos((1-i)u + jv) \\ \sin v \cos((1-i)u + jv) \\ \sin((1-i)u + jv) \end{pmatrix}, \quad (6.12)$$

where the non-zero coefficients are

$$\begin{aligned} \delta_{-1,-1} &= 0.17, & \delta_{-1,0} &= 0.11, & \delta_{0,0} &= 1, \\ \delta_{1,0} &= 4.5, & \delta_{2,0} &= -0.25, & \delta_{0,1} &= 0.01, \\ & & \delta_{2,1} &= -0.45. \end{aligned} \quad (6.13)$$

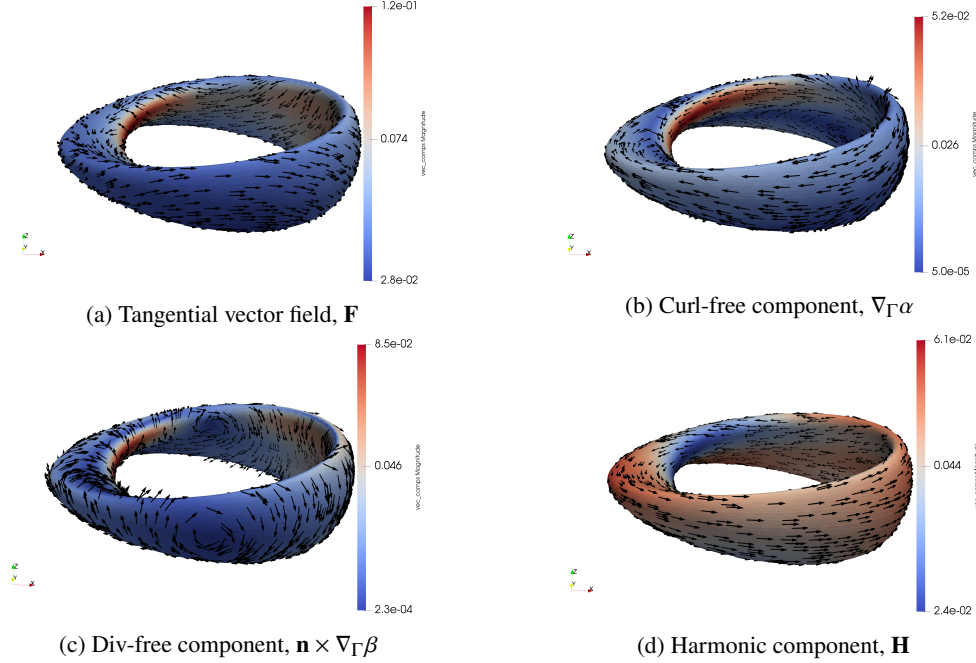


Figure 2: Hodge decomposition on a twisted torus with initial field  $\mathbf{V}$  given by a point current source at  $\mathbf{x}_0$ . The color bar represents the magnitude of the vector field and the arrows represent the direction of the field.

For this example, we define  $\mathbf{V} = \boldsymbol{\ell} \times (\mathbf{x} - \mathbf{x}_0) / |\mathbf{x} - \mathbf{x}_0|^3$ , with  $\mathbf{x}_0 = (0.2, 0.2, 0.2)$  and  $\boldsymbol{\ell} = (0, 1, 1)$  and then define  $\mathbf{F} = -\mathbf{n} \times \mathbf{n} \times \mathbf{V}$ . In Figure 2, we plot the tangential vector field  $\mathbf{F}$ , its curl-free component, its divergence-free component and the harmonic vector field  $\mathbf{H}$ . The second linearly independent harmonic vector field can be obtained by computing  $\mathbf{n} \times \mathbf{H}$ . The surface was discretized using  $N_{\text{patches}} = 600$  patches of order  $p = 9$ . In Table 4, we tabulate the results of a convergence study. We estimate the error in the computation of the harmonic vector fields by computing the  $\mathbb{L}^2$  norms of  $\nabla_\Gamma \cdot \mathbf{H}$  and  $\nabla_\Gamma \cdot (\mathbf{n} \times \mathbf{H})$  using spectral differentiation. For this example  $\|\mathbf{H}\| \approx 0.62498$ , so the above error estimate serves as a proxy for a relative error estimate as well. We observe the surface divergence and surface curl converge to zero as indicated in Table 4.

We also compute the 20 linearly independent harmonic vector fields on a genus 10 surface. For this geometry, we choose a random surface vector field  $\mathbf{V}$  whose components are random tensor product Legendre polynomials as discussed in Section 5. In Figure 3, we plot the surface along with these 20 linearly independent harmonic vector fields computed using our solver. The geometry was discretized using  $N_{\text{patches}} = 2160$  patches of order  $p = 9$ . As before, we verify the computations by calculating the  $\mathbb{L}^2$  norms of the surface divergence of  $\mathbf{H}$  and  $\mathbf{n} \times \mathbf{H}$ , where  $\mathbf{H}$  is the computed

$p$	$N_{\text{patches}}$	$N$	$\ \nabla_\Gamma \cdot \mathbf{H}\ _{\mathbb{L}^2(\Gamma)}$	$\ \nabla_\Gamma \cdot (\mathbf{n} \times \mathbf{H})\ _{\mathbb{L}^2(\Gamma)}$
9	150	6750	$1.4 \times 10^{-1}$	$1.1 \times 10^{-1}$
9	600	27 000	$1.4 \times 10^{-2}$	$1.0 \times 10^{-2}$
9	2400	108 000	$3.2 \times 10^{-4}$	$1.2 \times 10^{-4}$
9	9600	432 000	$1.8 \times 10^{-6}$	$8.5 \times 10^{-7}$

Table 4: Error in the surface divergence of  $\mathbf{H}$  and  $\mathbf{n} \times \mathbf{H}$  for the computed harmonic vector field on the twisted torus.

$p$	$N_{\text{patches}}$	$N$	$\ \nabla_{\Gamma} \cdot \mathbf{H}\ _{\mathbb{L}^2(\Gamma)}$	$\ \nabla_{\Gamma} \cdot \mathbf{n} \times \mathbf{H}\ _{\mathbb{L}^2(\Gamma)}$
9	2160	97 200	$5.6 \times 10^{-1}$	$1.4 \times 10^{-1}$
9	8640	388 800	$6.1 \times 10^{-3}$	$1.5 \times 10^{-3}$
9	34 560	1 555 200	$9.6 \times 10^{-5}$	$4.5 \times 10^{-5}$

Table 5: Error in the surface divergence of  $\mathbf{H}$  and  $\mathbf{n} \times \mathbf{H}$  for one of the computed harmonic vector fields on the genus 10 geometry. The computed harmonic vector field had  $\mathbb{L}^2$  norm of 0.66

harmonic field and observing that they converge to zero. In Table 5, we tabulate convergence results for a harmonic vector field on the genus 10 surface computed using our solver.

## 7 Conclusions and future work

In this paper, we have presented a high-order FMM-accelerated iterative solver for the numerical solution of the Laplace-Beltrami equation on complex smooth surfaces in three dimensions. The Laplace-Beltrami problem  $\Delta_{\Gamma}\psi = f$  is converted to a second-kind integral equation by representing the solution as  $\psi = \mathcal{S}[\sigma]$  or  $\psi = \mathcal{S}^2[\sigma]$ , and using appropriate Caldéron identities. The resulting integral equation, which requires the application of various Laplace layer potentials, is then discretized using a high-order method with locally corrected quadratures for computing the weakly-singular layer potentials; their application is accelerated using fast multipole methods.

While the integral equation can be written in several equivalent analytic forms, we demonstrate the necessity of maintaining numerical second-kindness by explicitly isolating the identity term of the Fredholm equation in order to avoid stagnation of iterative solvers such as GMRES. In some of these equivalent formulations, the discretized operator ends up having a high-dimensional spurious null space (proportional to the number of patches used). This issue is related to the difficulty of directly discretizing the differential form of the Laplace-Beltrami equation when using patch-based discretizations of surfaces and not enforcing smoothness across patches. However, both of these issues can be mitigated by explicitly isolating the identity part of the Fredholm equation.

Finally, we also presented numerical examples demonstrating the computation of harmonic vector fields on surfaces using the Laplace-Beltrami solver. These vector fields are both of pure mathematical interest and are also required for solving problems in type I superconductivity and electromagnetism on topologically non-trivial geometries.

There are still several open questions that remain to be addressed. These include coupling high-order discretizations of the Laplace-Beltrami integral equations to fast direct solvers; subsequently using these solvers to develop iterative solvers for the solution of Maxwell’s equations using the generalized Debye formulation; and extending these ideas for the solution of surface diffusion problems that arise in pattern formation and cell biology. These are all ongoing areas of research.

## References

- [1] E. Bänsch, P. Morin, and R. H. Nochetto. A finite element method for surface diffusion: the parametric case. *Journal of Computational Physics*, 203(1):321–343, 2005.

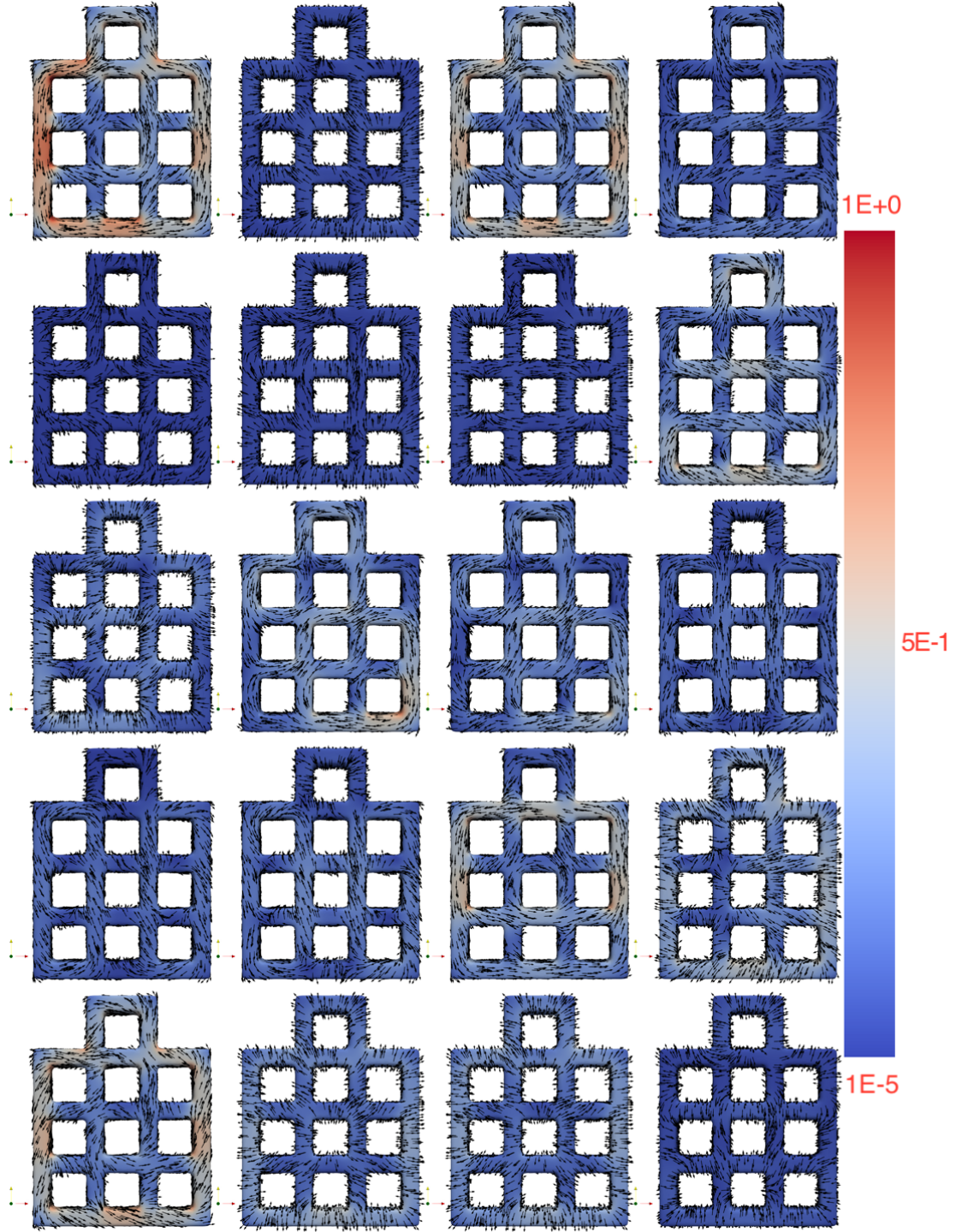


Figure 3: The 20 harmonic fields computed on a genus 10 geometry which was discretized with  $N_{\text{patches}} = 2160$  of order  $p = 9$ . The initial tangential vector field in each case is normalized to have  $\|\mathbf{F}\|_{\mathbb{L}^2(\Gamma)} = 1$ . The surface divergence of calculated harmonic field  $\mathbf{H}$  in each case is  $\|\nabla_{\Gamma} \cdot \mathbf{H}\|_{\mathbb{L}^2(\Gamma)} \approx O(10^{-1})$  and surface curl is  $\|\nabla_{\Gamma} \cdot \mathbf{n} \times \mathbf{H}\|_{\mathbb{L}^2(\Gamma)} \approx O(10^{-1})$ . The color bar represents the magnitude of the vector field and the arrows represent the direction of the field.



- [2] L. Beirão da Veiga, F. Brezzi, L. D. Marini, and A. Russo. The hitchhiker’s guide to the virtual element method. *Mathematical models and methods in applied sciences*, 24(08):1541–1573, 2014.
- [3] M. Bertalmio, L.-T. Cheng, S. Osher, and G. Sapiro. Variational problems and partial differential equations on implicit surfaces. *Journal of Computational Physics*, 174(2):759–780, 2001.
- [4] A. Bonito, A. Demlow, and R. H. Nochetto. Finite element methods for the laplace–beltrami operator. In *Handbook of Numerical Analysis*, volume 21, pages 1–103. Elsevier, 2020.
- [5] J. Bremer. On the Nyström discretization of integral equations on planar curves with corners. *Appl. Comput. Harm. Anal.*, 32:45–64, 2012.
- [6] E. Burman, P. Hansbo, M. G. Larson, and A. Massing. A cut discontinuous Galerkin method for the Laplace–Beltrami operator. *IMA Journal of Numerical Analysis*, 37(1):138–169, 2017.
- [7] Y. Chen and C. B. Macdonald. The closest point method and multigrid solvers for elliptic equations on surfaces. *SIAM Journal on Scientific Computing*, 37(1):A134–A155, 2015.
- [8] H. Contopanagos, B. Dembart, M. Epton, J. J. Ottusch, V. Rokhlin, J. L. Visser, and S. M. Wandzura. Well-conditioned boundary integral equations for three-dimensional electromagnetic scattering. *IEEE Trans. Antennas Propag.*, 50(12):1824–1830, 2002.
- [9] Q. I. Dai, W. C. Chew, L. J. Jiang, and Y. Wu. Differential-Forms-Motivated Discretizations of Electromagnetic Differential and Integral Equations. *IEEE Ant. Wire. Propag. Lett.*, 13:1223–1226, 2014.
- [10] A. Demlow and G. Dziuk. An adaptive finite element method for the Laplace–Beltrami operator on implicitly defined surfaces. *SIAM Journal on Numerical Analysis*, 45(1):421–442, 2007.
- [11] C. Epstein and L. Greengard. Debye sources and the numerical solution of the time harmonic Maxwell equations. *Commun. Pure Appl. Math.*, 63(4):413–463, 2010.
- [12] C. L. Epstein, Z. Gimbutas, L. Greengard, A. Klöckner, and M. O’Neil. A consistency condition for the vector potential in multiply-connected domains. *IEEE Trans. Magn.*, 49(3):1072–1076, 2013.
- [13] C. L. Epstein and L. Greengard. Debye sources and the numerical solution of the time harmonic Maxwell equations. *Communications on Pure and Applied Mathematics: A Journal Issued by the Courant Institute of Mathematical Sciences*, 63(4):413–463, 2010.
- [14] C. L. Epstein, L. Greengard, and M. O’Neil. Debye sources and the numerical solution of the time harmonic maxwell equations II. *Communications on pure and applied mathematics*, 66(5):753–789, 2013.
- [15] C. L. Epstein and M. Rachh. Debye source representation for type-I superconductors, I, 2021.
- [16] FMM3D. <https://github.com/flatironinstitute/fmm3d>. *GitHub Repository*.
- [17] FMM3DBIE. <https://gitlab.com/fastalgorithms/fmm3dbie>. *GitHub Repository*.

- [18] T. Frankel. *The Geometry of Physics*. Cambridge University Press, New York, NY, 2011.
- [19] M. Frittelli and I. Sgura. Virtual element method for the Laplace-Beltrami equation on surfaces. *ESAIM: Mathematical Modelling and Numerical Analysis*, 52(3):965–993, 2018.
- [20] T. Goodwill and M. O’Neil. On the numerical solution of the Laplace-Beltrami problem on piecewise-smooth surfaces. *arXiv preprint arXiv:2108.08959*, 2021.
- [21] L. Greengard, M. O’Neil, M. Rachh, and F. Vico. Fast multipole methods for the evaluation of layer potentials with locally-corrected quadratures. *Journal of Computational Physics: X*, 10:100092, 2021.
- [22] L. Greengard and V. Rokhlin. A new version of the Fast Multipole Method for the Laplace equation in three dimensions. *Acta Numerica*, 6:229–269, 1997.
- [23] J. B. Greer, A. L. Bertozzi, and G. Sapiro. Fourth order partial differential equations on general geometries. *Journal of Computational Physics*, 216(1):216–246, 2006.
- [24] L.-M. Imbert-Gerard and L. Greengard. Pseudo-Spectral Methods for the Laplace-Beltrami equation and the Hodge decomposition on Surfaces of Genus One. *Numer. Methods Partial. Differ. Equ.*, 33(3):941–955, 2017.
- [25] J. Jost. *Riemannian geometry and geometric analysis*. Springer Verlag, 2011.
- [26] H. Kim, A. Yun, S. Yoon, C. Lee, J. Park, and J. Kim. Pattern formation in reaction–diffusion systems on evolving surfaces. *Computers & Mathematics with Applications*, 80(9):2019–2028, 2020.
- [27] T. Koornwinder. Two-variable analogues of the classical orthogonal polynomials. In *Theory and application of special functions (Proc. Advanced Sem., Math. Res. Center, Univ. Wisconsin, Madison, Wis., 1975)*, pages 435–495. Academic Press New York, 1975.
- [28] R. Kress. *Linear Integral Equations*. Springer, New York, NY, 2014.
- [29] J. Kromer and D. Bothe. Highly accurate numerical computation of implicitly defined volumes using the Laplace-Beltrami operator. *arXiv preprint arXiv:1805.03136*, 2018.
- [30] M. C. A. Kropinski and N. Nigam. Fast integral equation methods for the Laplace-Beltrami equation on the sphere. *Adv. Comput. Math.*, 40(2):577–596, 2014.
- [31] M. C. A. Kropinski, N. Nigam, and B. Quaife. Integral equation methods for the Yukawa-Beltrami equation on the sphere. *Advances in Computational Mathematics*, 42(2):469–488, 2016.
- [32] C. B. Macdonald and S. J. Ruuth. Level set equations on surfaces via the closest point method. *Journal of Scientific Computing*, 35(2):219–240, 2008.
- [33] C. B. Macdonald and S. J. Ruuth. The implicit closest point method for the numerical solution of partial differential equations on surfaces. *SIAM Journal on Scientific Computing*, 31(6):4330–4350, 2010.

- [34] D. Malhotra, A. Cerfon, L.-M. Imbert-Gérard, and M. O’Neil. Taylor states in stellarators: A fast high-order boundary integral solver. *Journal of Computational Physics*, 397:108791, 2019.
- [35] J. Nedelec. *Acoustic and Electromagnetic Equations*. Springer, New York, NY, 2001.
- [36] F. Olver, D. Lozier, R. Boisvert, and C. Clark. NIST handbook of mathematical functions. *1st edn. Cambridge University Press, New York*, 2010.
- [37] M. O’Neil. Second-kind integral equations for the Laplace-Beltrami problem on surfaces in three dimensions. *Adv. Comput. Math.*, 44(5):1385–1409, 2018.
- [38] C. H. Papas. *Theory of Electromagnetic Wave Propagation*. Dover, New York, NY, 1988.
- [39] R. G. Plaza, F. Sanchez-Garduno, P. Padilla, R. A. Barrio, and P. K. Maini. The effect of growth and curvature on pattern formation. *Journal of Dynamics and Differential Equations*, 16(4):1093–1121, 2004.
- [40] A. Rahimian, I. Lashuk, S. Veerapaneni, A. Chandramowlishwaran, D. Malhotra, L. Moon, R. Sampath, A. Shringarpure, J. Vetter, R. Vuduc, et al. Petascale direct numerical simulation of blood flow on 200k cores and heterogeneous architectures. In *SC’10: Proceedings of the 2010 ACM/IEEE International Conference for High Performance Computing, Networking, Storage and Analysis*, pages 1–11. IEEE, 2010.
- [41] S. Rosenberg. *The Laplacian on a Riemannian Manifold*. Cambridge University Press, 1997.
- [42] Y. Saad and M. H. Schultz. GMRES: A Generalized Minimal Residual Algorithm for Solving Nonsymmetric Linear Systems. *SIAM J. Sci. Stat. Comput.*, 7:856–869, 1986.
- [43] J. Sifuentes, Z. Gimbutas, and L. Greengard. Randomized methods for rank-deficient linear systems. *Elec. Trans. Num. Anal.*, 44:177–188, 2015.
- [44] S. K. Veerapaneni, A. Rahimian, G. Biros, and D. Zorin. A fast algorithm for simulating vesicle flows in three dimensions. *J. Comput. Phys.*, 230:5610–5634, 2011.
- [45] F. Vico, L. Greengard, and Z. Gimbutas. Boundary integral equation analysis on the sphere. *Numer. Math.*, 128:463–487, 2014.
- [46] F. Vico, L. Greengard, M. O’Neil, and M. Rachh. A fast boundary integral method for high-order multiscale mesh generation. *SIAM J. Sci. Comput.*, 42(2):A1380–A1401, 2020.
- [47] B. Vioreanu and V. Rokhlin. Spectra of Multiplication Operators as a Numerical Tool. *SIAM J. Sci. Comput.*, 36:A267–A288, 2014.
- [48] M. Wang, S. Leung, and H. Zhao. Modified virtual grid difference for discretizing the laplace–beltrami operator on point clouds. *SIAM Journal on Scientific Computing*, 40(1):A1–A21, 2018.